



Research Paper

Genomic characterization reveals novel mechanisms underlying the valosin-containing protein-mediated cardiac protection against heart failure

Ning Zhou^{a,b,1}, Xin Chen^{c,1}, Jing Xi^{a,1}, Ben Ma^{a,e}, Christiana Leimena^a, Shaunrick Stoll^a, Gangjian Qin^d, Charles Wang^{c,**}, Hongyu Qiu^{a,e,*}

^a Division of Physiology, Department of Basic Sciences, School of Medicine, Loma Linda University, Loma Linda, CA, 92350, USA

^b Division of Cardiology, Department of Internal Medicine, Tongji Hospital, Tongji Medical College, Huazhong University of Science and Technology, Wuhan, 430000, China

^c Center for Genomics & Department of Basic Sciences, School of Medicine, Loma Linda University, Loma Linda, CA, 92350, USA

^d Department of Biomedical Engineering, School of Medicine and School of Engineering, University of Alabama at Birmingham, Birmingham, AL, 35294, USA

^e Center of Molecular and Translational Medicine, Institution of Biomedical Science, Georgia State University, Atlanta, GA, 30303, USA



ARTICLE INFO

Keywords:

Valosin-containing protein
Cardiac hypertrophy
Heart failure
Pressure overload
RNA sequencing

ABSTRACT

Chronic hypertension is a key risk factor for heart failure. However, the underlying molecular mechanisms are not fully understood. Our previous studies found that the valosin-containing protein (VCP), an ATPase-associated protein, was significantly decreased in the hypertensive heart tissues. In this study, we tested the hypothesis that restoration of VCP protected the heart against pressure overload-induced heart failure. With a cardiac-specific transgenic (TG) mouse model, we showed that a moderate increase of VCP was able to attenuate chronic pressure overload-induced maladaptive cardiac hypertrophy and dysfunction. RNA sequencing and a comprehensive bioinformatic analysis further demonstrated that overexpression of VCP in the heart normalized the pressure overload-stimulated hypertrophic signals and repressed the stress-induced inflammatory response. In addition, VCP overexpression promoted cell survival by enhancing the mitochondria resistance to the oxidative stress via activating the Rictor-mediated-gene networks. VCP was also found to be involved in the regulation of the alternative splicing and differential isoform expression for some genes that are related to ATP production and protein synthesis by interacting with long no-coding RNAs and histone deacetylases, indicating a novel epigenetic regulation of VCP in integrating coding and noncoding genomic network in the stressed heart. In summary, our study demonstrated that the rescuing of a deficient VCP in the heart could prevent pressure overload-induced heart failure by rectifying cardiac hypertrophic and inflammatory signaling and enhancing the cardiac resistance to oxidative stress, which brought in novel insights into the understanding of the mechanism of VCP in protecting patients from hypertensive heart failure.

1. Introduction

Heart failure is a leading cause of death, of which hypertension is one of the major risk factors [1,2]. Persistent high blood pressure (BP) in chronic hypertensive patients increases the left ventricular (LV) afterload and subsequently changes the structures of LV, which is also known

as remodeling, eventually resulting in impaired myocardial performance, leading to heart failure [1,3]. Despite intensive research efforts over several decades [4–6], the molecular mechanisms underlying the hypertensive heart failure remain largely unknown.

The valosin-containing protein (VCP) belongs to the type II class of the AAA (ATPases Associated with various cellular Activities) ATPase

* Corresponding author. Center of Molecular and Translational Medicine, Institution of Biomedical Science, Georgia State University, Petit Research Center, Room 588, 100 Piedmont Ave, Atlanta, GA, 30303, USA.

** Corresponding author. Center for Genomics, Department of Basic Sciences, School of Medicine, Loma Linda University, 11021 Campus Street, AH 120/104, Loma Linda, CA, 92350, USA.

E-mail addresses: chwang@llu.edu (C. Wang), hqiu@gsu.edu (H. Qiu).

¹ Equal contributions.

<https://doi.org/10.1016/j.redox.2020.101662>

Received 11 May 2020; Received in revised form 20 July 2020; Accepted 26 July 2020

Available online 30 July 2020

2213-2317/© 2020 The Author(s).

Published by Elsevier B.V. This is an open access article under the CC BY-NC-ND license

(<http://creativecommons.org/licenses/by-nc-nd/4.0/>).

family [7–9], and has been associated with a wide variety of essential intracellular pathways in cancer cells [10–12]. Clinical studies found that VCP mutations have been associated with cardiomyopathy in humans and other species [13]. Cardiac-specific overexpression of an enzymatically mutated VCP (VCPK524A) in a transgenic mouse led to the development of cardiomyopathy [14]. In addition, knockdown of TER94 (VCP homolog in *Drosophila*) with cardiac-restricted siRNA severely disrupted myofibrillar organization and heart function in adult flies [15]. Taken together, these findings highlight the importance of VCP in the heart. Our previous studies have characterized VCP expression in the heart *in vivo* and in cardiomyocytes *in vitro* [16] and demonstrated a remarkable association between the VCP expression with hypertensive heart disease (HHD). VCP expression was found to be significantly reduced in the hearts of spontaneously hypertensive rats (SHRs) compared to their normotensive controls [17]. In addition, VCP expression was detected to be progressively decreased in the mouse hearts under persistent pressure overload caused by a prolonged transverse aortic constriction (TAC) [17]. These data imply that a deficiency of VCP in the hearts is correlated with the development of cardiac pathogenesis under the pressure overload. Thus, we hypothesized that restoration of VCP in the hypertensive heart would prevent pressure overload-induced heart failure.

In this study, using a transgenic (TG) mouse model in which VCP was specifically overexpressed in the heart, we tested whether an increased VCP in the heart prevents pressure overload-induced heart failure by comparing VCP TG mice with the wild type (WT) controls in terms of the physiological and histological alterations in cardiac structure and function. In addition, RNA sequencing (RNA-seq) and a comprehensive analysis were performed to identify the genes specifically regulated by VCP in the heart upon the chronic pressure overload, including differentially expressed genes (DEG), signaling pathways and upstream regulators as well as gene splicing alterations. Our results brought to light the new molecular mechanisms by which VCP protects the heart against hypertensive heart failure.

2. Materials and methods

Animal Models. A cardiac-specific VCP TG mouse model (FVB) was generated with an alpha MHC promoter, as described previously [17, 18], in which the VCP was shown an average of 3.5-fold increase in the heart tissues compared with their litter-matched WT mice [17,18]. There are no significant differences between the VCP TG and WT mice at the baseline condition at the ages of three to six-months old [17,18]. No difference was found between male and female mice in both groups at this age.

2 to 4-month old VCP TG and their litter-matched WT male mice, were used in this study. The animal numbers for each study were detailed in the figure legend. All animal procedures were performed in accordance with the NIH guidance (Guide for the Care and Use of Laboratory Animals, revised 2011) and the protocols were approved by the Institutional Animal Care and Use Committee of Loma Linda University.

Surgical procedures. Both VCP TG and WT mice were randomly assigned into two experimental groups, sham or TAC for 5 weeks (5 W). TAC was performed to induce pressure overload on the heart as previously described [17,19]. Mice were anesthetized by inhalation of 2% isoflurane. The transverse aorta was isolated, and a blunted 27-gauge needle was tied to the aorta between the origins of the innominate artery and left common carotid artery, and then removed to yield a constriction. The sham-operated mice underwent the same procedure except for constriction of the aorta [17].

Echocardiography and hemodynamic measurements. Physiological measurements were performed *in vivo* at the end of 5 W TAC under anesthesia with 2% isoflurane, the same as previous [17]. Cardiac function and morphology were determined in mice by echocardiography using a GE Logiq E vet machine with a 13-MHz probe as described previously [17]. A Millar catheter (SPR-671; Millar Instruments)

connected to a Power Laboratory System (AD Instruments, Castle Hill, Australia) was used for the hemodynamic analysis [17,19].

Histological analysis: Mice were euthanized with carbon dioxide inhalation after the hemodynamic measurements and the heart tissues were collected for *ex vivo* histological and molecular studies. The mouse hearts, LV and lung tissues were weighted and normalized with body weight. The cross-sectional area (CSA) of the myocyte and collagen contents were determined in LV tissue section as described previously [17,19]. The myocardial apoptosis was measured by terminal deoxynucleotidyl transferase dUTP nick end labeling (TUNEL) according to the manufacturer's instructions (Roche Applied Science, South San Francisco, CA, USA) [17,19]. In addition, ROS indicators, including 8-hydroxydeoxyguanosine (8-OHdG), 4 hydroxy-2-noneal (4HNE), malondialdehyde (MDA) were measured by immunofluorescent staining with a minor modified method as described [20–22].

Protein extraction and western blotting: Total proteins extracted from LV tissues were measured by western blotting and detected using the LI-COR Odyssey Infrared Imaging System (LI-COR Biosciences, Lincoln, NE, USA) as described previously [17,19]. GAPDH was used for a loading control of the total proteins.

RNA extraction and RNA-seq. Total RNA was extracted from left ventricular (LV) tissues using Qiagen miRNeasy kit. NuGen Ovation Mouse RNA-seq kit was used to construct RNA-seq libraries with 1% of Ambion's ERCC mix1 spike-in control. RNA-seq libraries were sequenced on Illumina HiSeq 4000 at the Loma Linda University Center for Genomics (150 × 2 bp paired-end reads). The RNA-seq data quality was assessed using the ERCC spiked-in control.

Real-time quantitative RT-PCR (q-PCR). cDNA was synthesized from RNA of each sample using the Transcriptor First Strand cDNA Synthesis Kit (Roche). q-PCR was performed on a CFX96 Touch Real-Time PCR Detection System by using iTaq Universal SYBR Green Supermix (Bio-Rad) according to the manufacturer's instructions [18, 23]. Each sample was performed in triplicate and the values were averaged.

2.1. Bioinformatic analysis of RNA-seq data

- **RNA sequencing and quality control (QC):** The next-generation sequencing (NGS) was used to determine the transcriptomic gene expression alteration modulated by VCP using RNA-seq. The raw Fastq data were assessed by FastQC (v0.11.4) and Bioconductor package ShortRead for quality control. The trimming process was performed by trimmomatic v0.35 [24] with the following options: LEADING:20 TRAILING:20 CROP:150 HEADCROP:4 SLIDING WINDOW:4:15 MINLEN:100. After trimming, we performed gene-level and transcript-level analyses, respectively. The mouse GRCh38 and Ensembl Musculus. v79 were used as reference genome and transcript annotation files for the following analysis.
- **Identification of differentially expressed genes (DEGs):** In the gene-level analysis, the trimmed fastq data were aligned to the reference genome and quantified by Kallisto v0.43.1 with default parameters. In Kallisto, isoform expression for each gene was summed to derive the counts and transcript per million (TPM) values by Bioconductor package tximport. The analysis of DEGs was performed with DESeq2. Genes <10 counts were discarded for DEG analysis. The DEGs were defined as the false discovery rate (FDR) < 0.05. In the transcript-level analysis, the trimmed fastq data were aligned by the 2-pass mode of STAR v2.5.4b [25] with default parameters.
- **Visualization of DEGs:** To visualize the DEGs, we performed a Principal Component Analysis (PCA) and a Hierarchical Clustering Analysis (HCA) by Partek Genomic Suite 6.0 with default options. Circos v 0.69–3 [26] was used to draw the fold change of DEGs under different comparisons.
- **Gene Ontology (GO) functional analysis:** GO analysis was performed by using a web-based tool GeneCodis [27–29]. Briefly, a statistical test, usually the hypergeometric, χ^2 , binomial, or Fisher's

exact test, is used to compute *p* values, which are subsequently adjusted for multiple testing. The result of this analysis is a list of single biological annotations from a given ontology with their corresponding *p*-values. Those terms with *p*-values indicating statistical significance are representative of the analyzed list of genes and can provide information about the underlying biologic processes. Graphs were generated by GraphPad Prism8 based on the GeneCodis data.

- **Pathway analysis:** Ingenuity Pathway Analysis (IPA) (QIAGEN Inc., <https://www.qiagenbioinformatics.com/products/ingenuity-pathway-analysis>) was employed for the assessment of biological and interaction networks of candidate genes. The candidate genes were uploaded into the IPA for the identification of their biological functions and the functional networks of the eligible molecules.
- **Alternative splicing analysis:** The analysis of differentially expressed transcripts (DETXs) was performed by LeafCutter [30] with the default parameter setting. A splicing event was identified if the FDR<0.05. LeafViz was used to visualize these significant splicing events.

Statistical analysis: Differences among the groups were determined by one way or two-way ANOVA followed by a post-hoc Tukey test. A value of *p* < 0.05 was considered significant.

3. Results

1. Overexpression of VCP attenuates the TAC-induced pathological cardiac remodeling in VCP TG mice

To determine the effect of VCP on the chronic pressure overload-induced cardiac remodeling, both WT and VCP TG adult mice were

submitted to TAC for 5 W and the pressure overload was confirmed by an increase of the aortic blood pressure (BP) before the banding site measured by an invasive cardiac catheter. As shown in Fig. 1A-B, compared with sham-operated mice, 5 W TAC increased aortic systolic and diastolic blood pressure (ASBP and ADBP) in both WT and VCP TG mice, indicating a successful establishment of cardiac pressure overload.

Cardiac echography was used to determine the structural alterations of the hearts of these mice (Fig. 1C). As shown in Fig. 1D-J, there was no significant difference in cardiac morphology between VCP TG and WT mice at sham-groups in terms of the wall thickness and LV diameter. At the end of 5 W TAC, WT mice developed a significant maladaptive cardiac hypertrophy, reflected by a notable increase of LV wall thickness which was represented by the posterior wall thickness at the end-diastole and systole (LVPWd and LVPWs) (Fig. 1D-E) and a dilation of LV chamber which was represented by an increase in LV internal diameter at end-diastole and systole (LVIDd, and LVIDs) (Fig. 1F-G).

This maladaptive hypertrophic remodeling was further confirmed in the 5 W TAC WT mice vs. sham controls by an increased LV mass represented by the ratio of LV weight to the body weight (Fig. 1H). In addition, the *ex vivo* histological studies on the LV tissue sections showed that, compared to the sham controls, at the end of 5 W TAC, WT mice exhibited a remarkable LV cardiomyocyte hypertrophy represented by the increased CSA (Fig. 1I) and a significant increase in fibrosis in LV tissues represented by the collagen contents (Fig. 1J). Furthermore, two hypertrophy-associated reprogram markers, *atrial natriuretic factor (ANF)* and *brain natriuretic factor (BNF)*, were significantly increased in the LV tissues in 5 W TAC mice compared to the sham controls (Fig. 1K). These cellular and molecular evidence further support the structural alterations observed by echography, indicating a pathological remodeling in the WT mice after 5 W TAC.

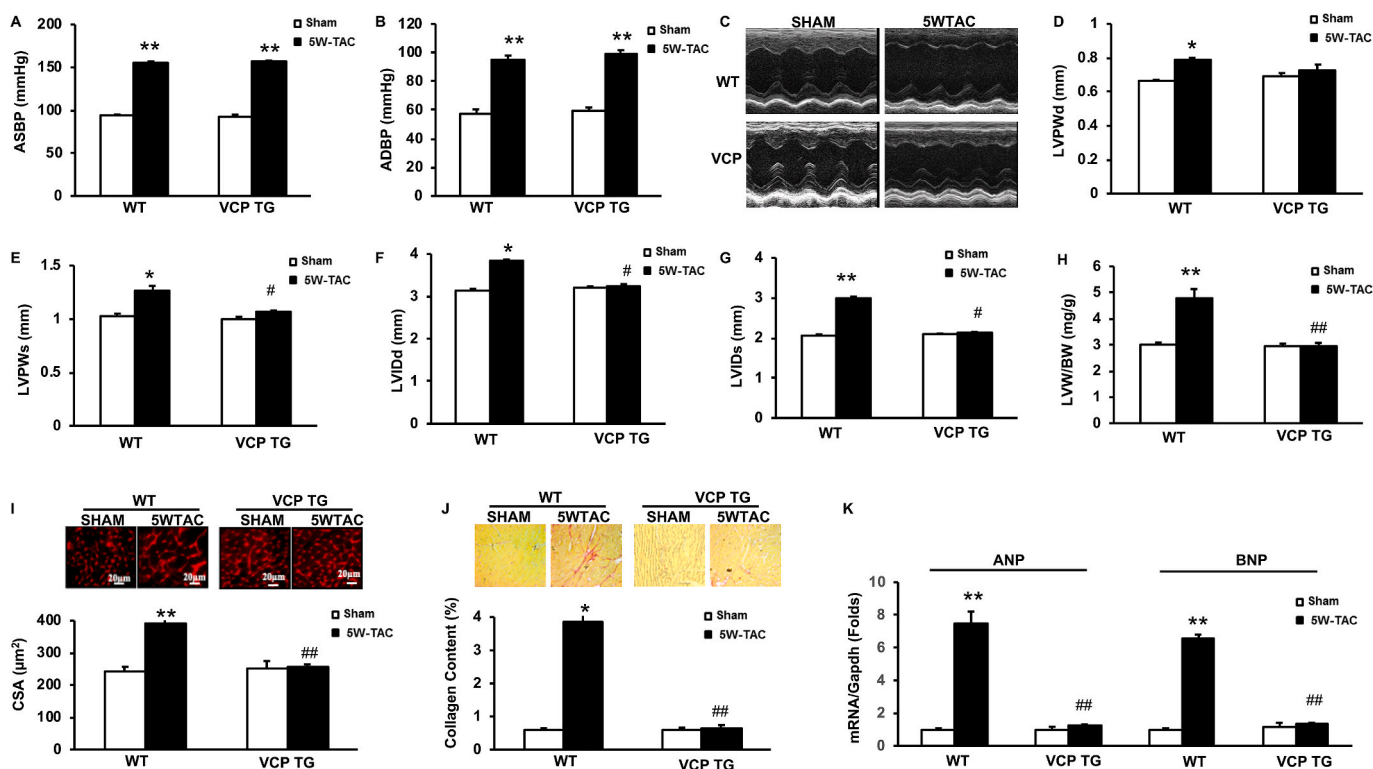


Fig. 1. Overexpression of VCP attenuates pressure-overload induced cardiac pathologic remodeling. The morphological alterations after 5 weeks (5 W) transverse aortic constriction (TAC) in both wild type (WT) and VCP transgenic (TG) mice vs sham. **A to B.** Alterations of aortic systolic and diastolic blood pressure (ASBP and ADBP) measured by invasive catheter *in vivo*. **C.** The representative images of echography. **D-E:** Left ventricular (LV) posterior wall thickness at end-diastole and systole (LVPWd and LVPWs). **F-G.** LV end diastolic and systolic dimension (LVEDd and LVEDs). **H.** LV weight normalized by body weights (LVW/BW). **I.** The representative images and quantitated cross-sectional areas (CSA) of cardiomyocytes in LV tissues. **J.** The representative images and quantitated collagen density in LV tissue sections. **K.** The mRNA levels of ANP and BNP normalized with GAPDH. **p* < 0.05, ***p* < 0.01 vs sham; #*p* < 0.05, ##*p* < 0.01 vs corresponding WT mice. N = 5 mice/group.

However, these pressure-overload-induced pathological cardiac remodelings were intriguingly attenuated in VCP TG mice at the end of 5 W TAC compared to their sham controls (Fig. 1C–K), in terms of the LV wall thickness and diameter, LV mass, cell size, fibrosis and hypertrophic markers. Since there was no significant difference in cardiac morphology between VCP TG and WT mice in the sham groups (Fig. 1C–K), these data indicated that VCP mediated a protective mechanism specifically against pathological cardiac remodeling caused by TAC.

2. Overexpression of VCP prevents the cardiac dysfunction caused by persistent pressure-overload

We next examined the effect of VCP on the cardiac function at the end of 5 W TAC by echography. Compared to the sham controls, WT mice showed an impaired contractile function at the end 5 W TAC, reflected by a decrease in LV ejection fraction (LVEF) (Fig. 2A), fractional shortening (FS) (Fig. 2B) and contractile index (Fig. 2C). The impaired LV function in these mice was also supported by the hemodynamic measurements via an invasive pressure catheter, represented by a subsequent increase in LV pressures at end of systole and diastole (LVESP and LVEDP) (Fig. 2D–E), and a significant decrease in the maximal and minimal rate of rise/descend of LV pressure (Max- and min-dp/dt) (Fig. 2F–G), when compared to their sham controls. In addition, the failed cardiac function of these mice was confirmed by a significant increase in the ratio of lung weight to body weight (LW/TL), which is a known index of heart failure (Fig. 2H), as compared to the sham WT mice. Furthermore, the histological studies showed a significant increase in the cell apoptosis measured by TUNEL in the TAC WT mouse hearts compared to their sham controls (Fig. 2I). This result further provided evidence of the cell damage accompanied with impaired cardiac dysfunction in the WT 5 W TAC mouse hearts. These data together

indicate that 5 W TAC induced LV dysfunction in WT mice reflected by the decreased contractile capability, impaired hemodynamics, and increased cell damage.

Remarkably, these cardiac functional deteriorations caused by the persistent pressure overload were not observed in VCP TG mice after 5 W TAC, indicating that overexpression of VCP in the heart prevents the pressure overload-induced impairment of cardiac function in VCP TG mice when compared to the WT TAC mice (Fig. 2A to I).

Together, these results suggested that persistent pressure-overload induced maladaptive cardiac hypertrophy and contractile dysfunction in WT mice. However, they were both relieved by the overexpression of VCP in the TG mice.

3. Rescue of VCP elicits a distinct transcriptome corresponding to the protection on the cardiac pathophysiological alterations caused by TAC

To explore the molecular basis of the protective effects by VCP, we compared the VCP expression in both TAC-treated VCP TG and WT mice to determine whether the physiological and histological alterations are correlated with the VCP expression in the hearts of these mice. As showed in Fig. 3A, 5 W TAC induced a dramatic decrease of VCP expression in the WT mouse hearts vs their sham controls, while the VCP level was preserved in the VCP TG mouse hearts at the post-TAC mice vs sham controls. This data indicated that the reduction of the VCP expression caused by TAC was rescued in TG mouse hearts.

Next, using the LV tissues derived from the same mice we observed above, we performed an RNA-seq followed by a comprehensive analysis to compare the cardiac transcriptomes between WT and VCP TG mice at the end of 5 W TAC. As shown in Fig. 3B, the PCA revealed a clear separation of transcriptomic profile between VCP TG and WT mouse groups at the end of 5 W TAC. HCA also displayed a distinct difference in

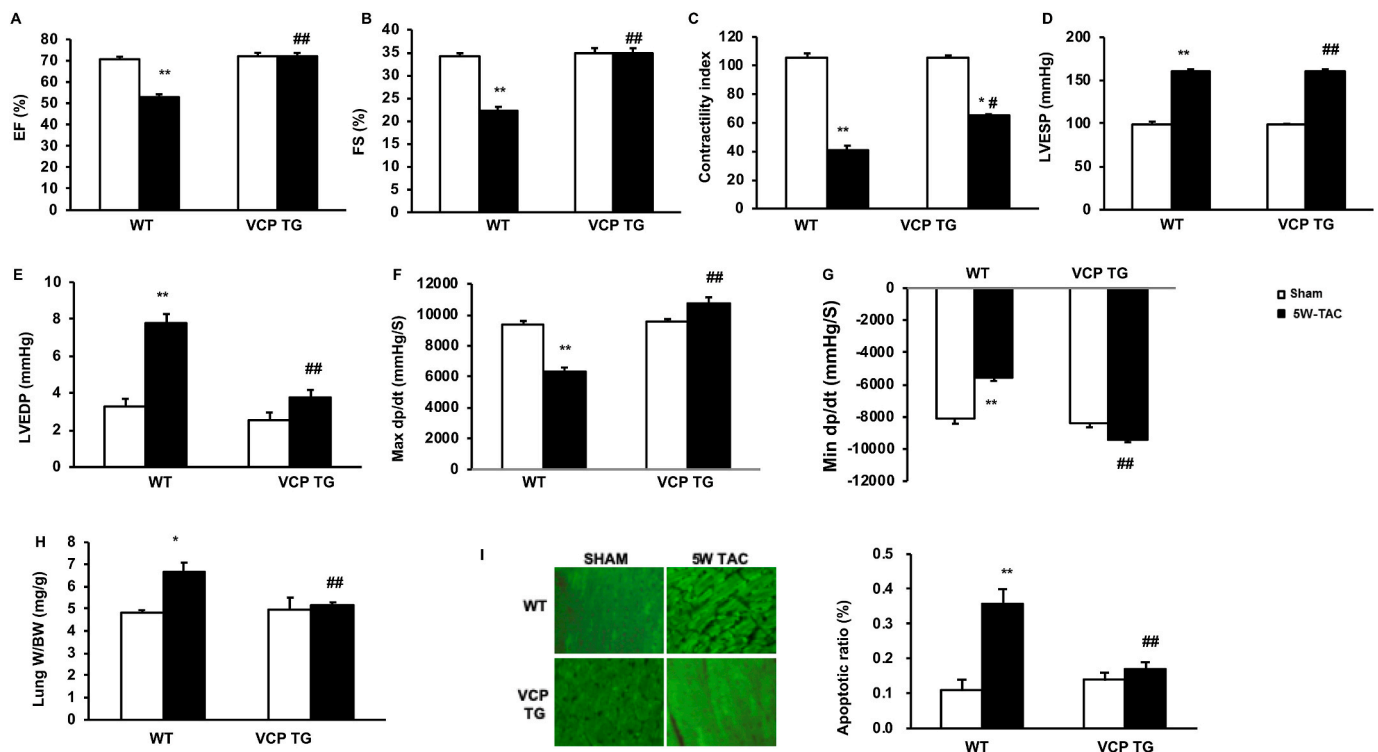


Fig. 2. Overexpression of the VCP prevents pressure-overload induced cardiac dysfunction. The alterations in cardiac function after 5 weeks (5 W) transverse aortic constriction (TAC) in both wild type (WT) and VCP transgenic (TG) mice vs sham. A–C. LV ejection fraction (EF), fractional shortening (FS), and contractile index in all the groups. D–E: LV end-systolic and -diastolic pressure (LVESP and LVEDP). F–G: The maximum or minimum rate of pressure (+dp/dt) in LV isovolumetric contraction. H. Lung weights normalized by body weights. I. The representative images and quantitated apoptosis ratio measured by histology *ex vivo* in LV tissues via TUNEL. * $p < 0.05$, ** $p < 0.01$ vs sham; # $p < 0.05$, ## $p < 0.01$ vs corresponding WT mice. $N = 5$ mice/group.

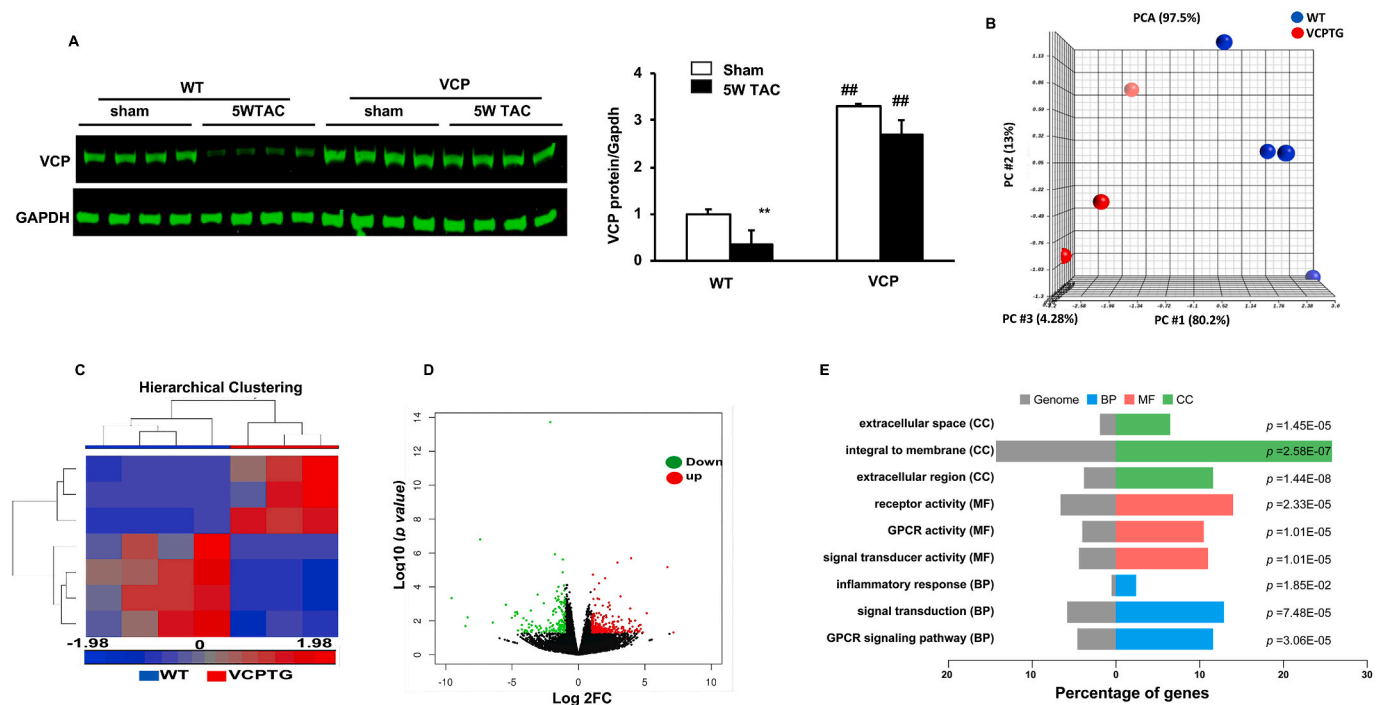


Fig. 3. VCP elicits a distinct stress-associated transcriptomic alteration in VCP TG mouse hearts vs WT mice at the end of 5 W TAC. **A.** VCP protein levels normalized to GAPDH. n = 4 mice/group. **B–C.** Profiles of RNA-seq analysis. Principal component analysis (PCA) (**B**) and Hierarchical clustering (**C**) of differentially expressed genes (DEGs) with FDR < 0.05. **D.** The volcano plot of DEGs based on based on the FC > 2 and p < 0.05 between WT and VCP TG mice at the end of 5 W TAC, in terms of the cellular components (CC), molecular function (MF) and biological process (BP) according to p-value. N = 3–4 mice/group for B–E. (For interpretation of the references to colour in this figure legend, the reader is referred to the Web version of this article.)

the whole transcriptome between the two TAC groups (Fig. 3C). Using p-value less than 0.05 and the fold change (FC) more than 2 as a threshold, we identified 448 DEGs between VCP TG and WT at the end of 5 W TAC, with 281 DEGs were upregulated and 167 DEGs were downregulated in VCP TG vs WT. The statistically significant genes that displayed large magnitude changes were visualized by a Volcano Plot combined with ANOVA test. Based on this analysis, a few of the DEGs were detected between the VCP TG and WT mice after 5 W TAC (Fig. 3D). As shown in Table 1, based on the fold changes, 19 out of 20 of the top genes are downregulated and only one gene was upregulated in VCP TG mice vs

Table 1
TOP DEGs between VCP TG vs WT after 5 W TAC (FDR = 0.05).

Gene names	FC
<i>Xist</i>	-15.82
<i>Pttg1</i>	-15.6
<i>Rpl29</i>	-10.13
<i>Rpph1</i>	-8.5
<i>Fosb</i>	-8.25
<i>Hist1h4c</i>	-5.13
<i>Hbb-b1</i>	-5.1
<i>H2-Aa</i>	-5.02
<i>Nr4a2</i>	-3.91
<i>Gpr75</i>	3.89
<i>Ptgs2</i>	-3.85
<i>Rpl34</i>	-3.42
<i>Nppa</i>	-3.27
<i>Phlda1</i>	-3.21
<i>Ccl2</i>	-3.17
<i>Cxcl1</i>	-3.07
<i>Fgf1</i>	-2.94
<i>Cyfp2</i>	-2.89
<i>Gdf15</i>	-2.76
<i>Slh</i>	-2.74

WT at the end of 5 W TAC. These top downregulated DEGs can be largely divided into three categories. One category includes the genes related to the protein synthesis and cell proliferation, growth and hypertrophy, such as *Ribosomal proteins (Rpl34, Rpl29)*, *Ribonuclease p RNA component H1 (Rpph1)*, *Fosb*, *Histone H4 (Hist1h4c)*, *Natriuretic peptide A (Nppa)*, *Fibroblast growth factor (FGF)*, and *Growth/differentiation factor 15 (Gdf15)*. The second category includes the genes involved in the cell apoptosis, such as *Securin (Pttg1)* and *Pleckstrin homology-like domain family A member 1 (Phlda1)*. The third category includes the genes related to the inflammation, such as *Prostaglandin-endoperoxide synthase 2 (Ptgs2)*, *Cytoplasmic FMR1 interacting protein 2 (Ccl2)* and *C-X-C Motif chemokine ligand 1 (Cxcl1)* and *Histocompatibility 2 (H2-Aa)*. In controversy, the upregulated top gene is the *Glucose-regulated protein 75 (Grp 75)* which involved in regulating the ER-mitochondrial coupling and oxidative stress.

GO functional analysis was also performed to classify the groups of these DEGs in terms of the cellular components (CC), molecular function (MF) and biological process (BP) according to p-value. As shown in Fig. 3E, when compared with WT 5 W TAC mice, the top enriched CC groups in VCP TG 5 W TAC mice were predominately involved in the integral membrane. The GO analysis based on the MF and BP showed a remarkable difference between the WT and VCP TG at the end of 5 W TAC that were related to GPCR signaling pathway (Fig. 3E).

These data together indicated that VCP TG mice exhibited distinct transcriptomic alterations from WT mice at the end of 5 W TAC, which is corresponding to the protective role of VCP in cardiac remodeling and dysfunction induced by TAC.

4. VCP represses the mitochondrial oxidative stress in the TAC-stressed heart.

The above results indicate a strong correlation between the VCP deficiency and the pathophysiological alterations at the end of 5 W TAC.

However, it remains unclear how the rescue of VCP attenuates the stress-induced deleterious signaling during the development of heart failure. To explore the underlying mechanisms, we first compared the 5 W TAC mouse hearts with their sham controls in WT mice to determine the TAC-induced gene alterations that contribute to the cardiac remodeling and dysfunction. Then, we determined the TAC-induced gene alterations in VCP TG mouse hearts, and finally, compared the difference of the gene regulation in response to 5 W TAC between the two groups.

As shown in Fig. 4A-B, the HCA results revealed that, compared to the corresponding sham control, there was a notable difference in 5 W TAC induced DEGs between WT and VCP TG mice. 1999 DEGs were detected in WT between 5 W TAC vs sham, among which more than 90% of the DEGs (1881 out of 1999) were downregulated and 10% of the DEGs were upregulated in 5 W TAC mice vs sham. Reciprocally, much fewer DEGs (682 vs 1999) were detected in VCP TG mice between 5 W TAC vs sham, among which DEGs were distributed in an even manner in both upregulated (342 out of 682) and downregulated (340 out of 682) changes in VCP TG TAC mice vs sham. In addition, some genes were regulated oppositely between WT and VCP TG during the development of heart failure (Table 2).

The GO analysis also showed a different pattern and enrichment between WT and VCP TG mice in response to the 5 W TAC (Fig. 4C and D). As compared to their corresponding sham controls, the top enriched CC groups were detected to be predominately involved in the membrane in WT 5 W TAC mice (Fig. 4C), while the top enriched CC of DEGs in VCP TG TAC were detected to be predominately involved in the mitochondria (Fig. 4D). Correspondingly, GO analysis based on MF and BP showed that most of DEGs between 5 W TAC vs sham in WT mice were associated with the receptor and signaling transducer activity and GPCR signaling pathway, whereas most of DEGs in VCP TG mice induced by 5 W TAC were associated with mitochondrial oxidative stress, protein binding, translation and anti-apoptosis (Fig. 4C–D).

We further conducted an IPA to identify the top upstream transcription factors that regulate the significant DEGs of each group. We

Table 2

The top DEGs between 5 W TAC vs sham in WT with a opposite change in VCP TG (by $p < 0.05$ and $FC > 2$).

Gene Name	Up in WT (FC)	Down in VCP TG (FC)	Gene Name	Down in WT (FC)	Up in VCP TG (FC)
<i>Nppa</i>	5.65	-21.75	<i>Gpr75</i>	-3.67	1.76
<i>Hbb-b1</i>	5.64	-15.10	<i>Klk1b26</i>	-3.43	2.77
<i>Mfap4</i>	3.85	-1.50	<i>Mt2</i>	-2.81	12.40
<i>Snca</i>	3.65	-11.87	<i>Vwa3a</i>	-2.66	2.13
<i>Egr3</i>	3.29	-1.58	<i>Slc10a6</i>	-2.59	2.28
<i>Dkk3</i>	2.97	-4.36	<i>Cyp26b1</i>	-2.53	2.00
<i>Nr4a2</i>	2.78	-3.76	<i>Lrg1</i>	-2.50	2.58
<i>Myl4</i>	2.54	-29.32	<i>Serpina3n</i>	-2.42	3.66
<i>Sln</i>	2.38	-84.45	<i>Lcn2</i>	-2.40	4.87
<i>Egr1</i>	2.31	-1.65	<i>Adh1</i>	-2.36	2.31
<i>Gdf15</i>	2.25	-2.22	<i>Spock2</i>	-2.30	2.35
<i>Ube2c</i>	2.24	-4.27	<i>Fam117b</i>	-2.29	2.49
<i>Col14a1</i>	2.21	-2.16	<i>Efnb3</i>	-2.26	1.50
<i>Rpp25</i>	2.17	-2.57	<i>Mt1</i>	-2.24	3.20
<i>Col3a1</i>	2.09	-1.70	<i>Fkbp5</i>	-2.15	5.97
<i>Fos</i>	2.08	-6.29	<i>Fas</i>	-2.13	2.23
<i>Myl7</i>	2.07	-25.54	<i>Arrdc2</i>	-2.09	4.20
<i>Ndr4</i>	2.06	-1.65	<i>Il4ra</i>	-2.08	3.16
<i>Cdh11</i>	2.01	-1.56	<i>Klhl2</i>	-2.02	1.82

found that the upstream regulators exhibited a difference between VCP TG and WT mice in response to TAC stress. *Interleukin 10 receptor subunit alpha (Il-10ra)*, a receptor for the cytokine IL10 that participates in anti-inflammatory functions, was identified as a key upstream regulator of the most DEGs in WT between 5 W TAC and sham mice and was predicted to be inhibited upon the 5 W TAC in WT mice (Fig. 5A), indicating a repression of the anti-inflammatory response in WT mice upon TAC. It is notable that this inhibition on the *Il-10ra*-mediated signaling was not detected in VCP TG TAC mice vs sham.

Reciprocally, a gene named *rapamycin-insensitive companion of mammalian target of rapamycin (Rictor)* was identified as a key upstream

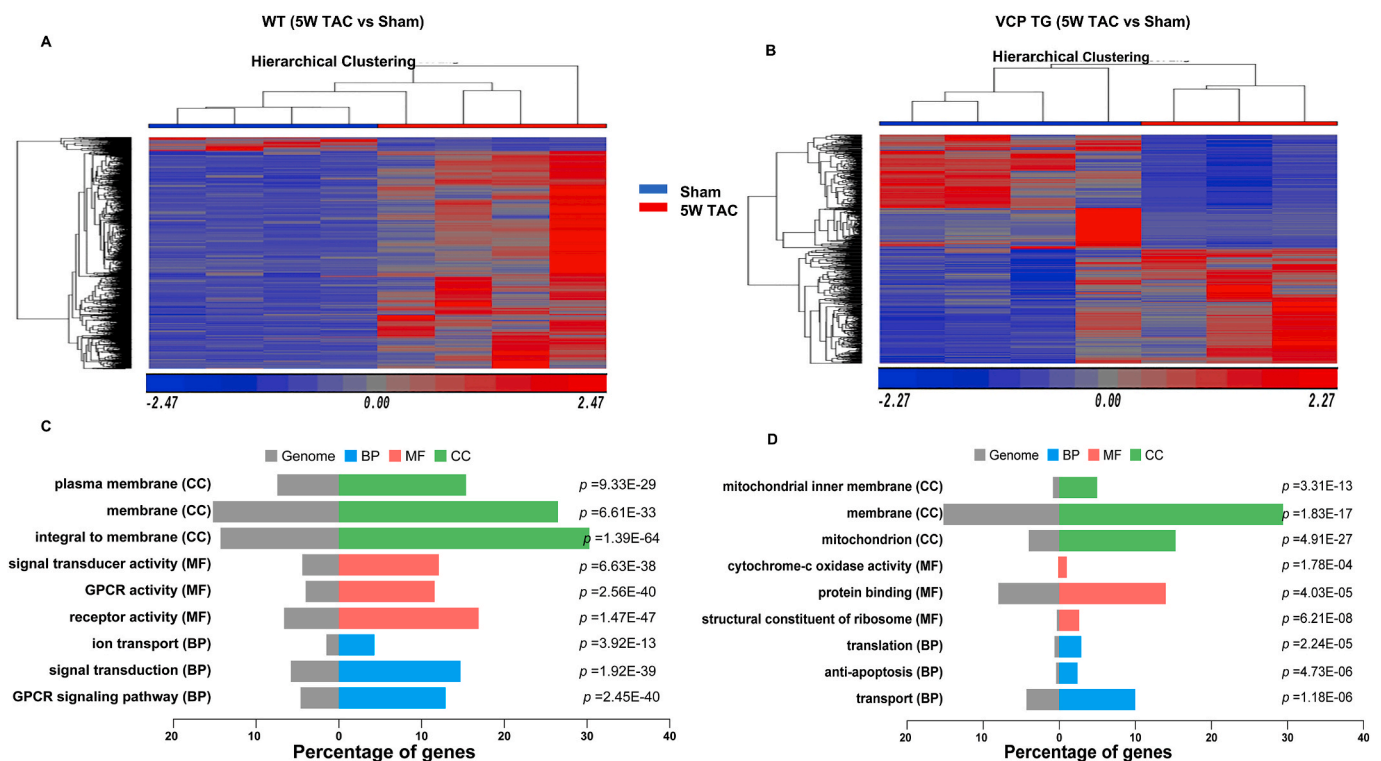


Fig. 4. Gene regulations were different between VCP TG and WT mice in response to TAC during the development of heart failure. Hierarchical clustering analysis (A–B) and GO functional analysis of DEGs (C–D) based on the comparison of 5 weeks (5 W) TAC vs sham in either WT (A and C) or VCP TG mice (B and D). CC: the cellular components; MF: the molecular function; and BP: biological process according to p -value. $N = 3-4$ mice/group.

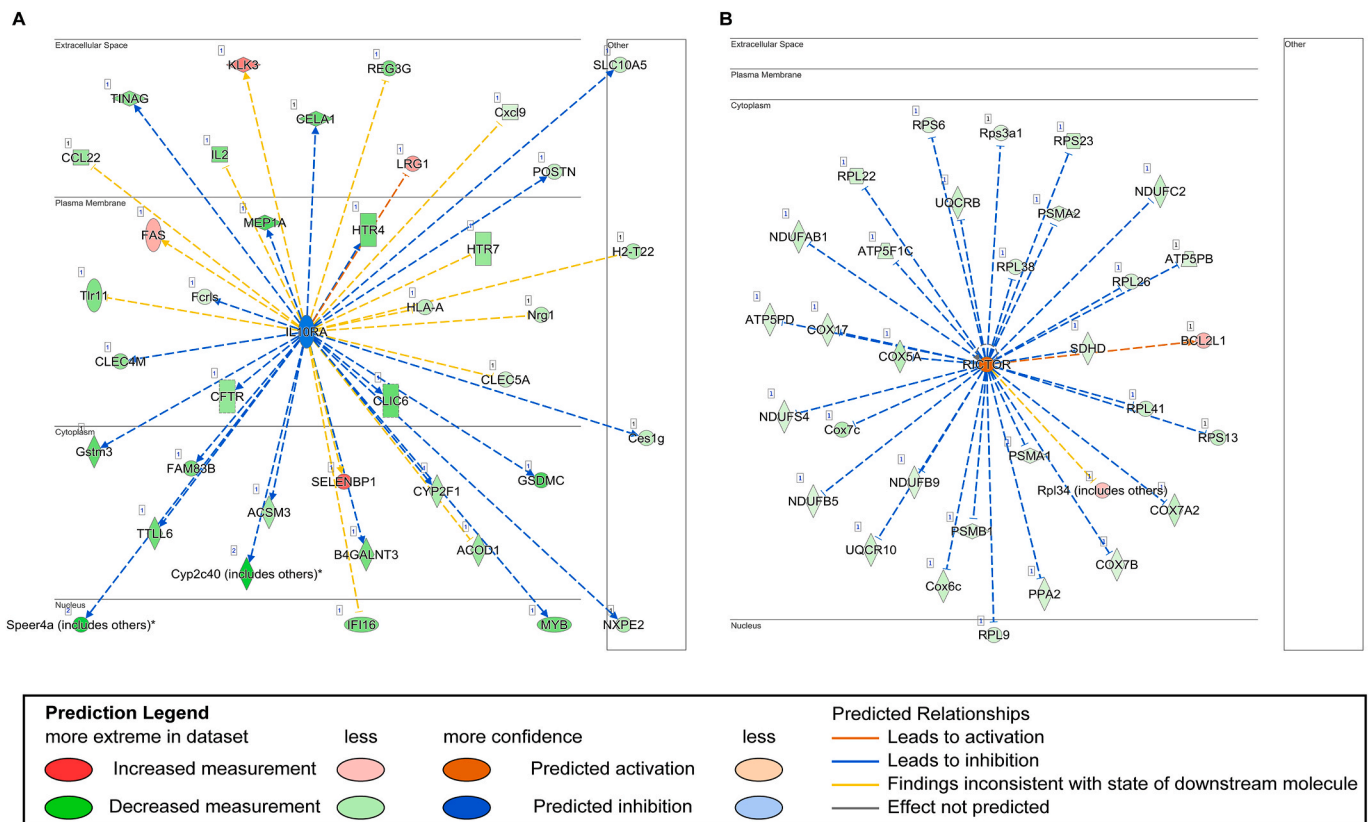


Fig. 5. VCP exhibits a different regulation on the transcription factors by an Ingenuity Pathway Analysis (IPA). **A.** *Il10-ra*-mediated downstream genes were inhibited in WT TAC mice as compared to their sham controls. **B.** *Rictor* was activated in VCP TG mice upon 5 W TAC, resulting in the repression of the downstream genes related to the oxidative stress. N = 3–4 mice/group.

regulator of the DEGs detected in VCP TG mice between TAC vs sham mice. As a key component of mTOR complex II (MTORC2) involved in the regulation of cell survival, *Rictor* was detected to be activated in VCP TG TAC mice, which resulted in significant downregulation of the mitochondrial genes that were related to the oxidative stress (Fig. 5B), including a group of supernumerary subunits of complex I or NADH-ubiquinone oxidoreductase (NDUFAB1, B5, B9, C2 and S4) and the subunits of complex III (ubiquinol cyt c reductase: UQCRC1, B, C, C1, C2, C3, C4, C5, C6, C7, C8, C9, C10, C11, C12, C13, C14, C15, C16, C17, C18, C19, C20, C21, C22, C23, C24, C25, C26, C27, C28, C29, C30, C31, C32, C33, C34, C35, C36, C37, C38, C39, C40, C41, C42, C43, C44, C45, C46, C47, C48, C49, C50, C51, C52, C53, C54, C55, C56, C57, C58, C59, C60, C61, C62, C63, C64, C65, C66, C67, C68, C69, C70, C71, C72, C73, C74, C75, C76, C77, C78, C79, C80, C81, C82, C83, C84, C85, C86, C87, C88, C89, C90, C91, C92, C93, C94, C95, C96, C97, C98, C99, C100) and complex IV (cytochrome c oxidase: COX 5A, 6C, A2, 7B, 7C, 17) and complex V (ATP5 PD, PB and F1c). Other genes belonged to the family of the ribosomal proteins L and S (RPL9,22, 26,41,38 and PRS 13,3a1,6 and 23) and proteasome genes (PSM A1, A2 and B1) were also found to be downregulated in VCP TG mice upon 5 W TAC vs sham (Fig. 5B).

We performed the qPCR to validate the alterations of the representative DEGs in Fig. 5B that were potentially associated with mitochondrial ROS production. As shown in Fig. 6A-C, the supernumerary subunits of complex I (*NdufAb1*, *C2* and *S4*) and the subunits of complex III (*Uqcrc10*) and complex IV (*Cox5a* and *Cox7c*) were significantly downregulated in VCP TG TAC mice, but not in WT mice.

In addition, we determined the oxidative stress levels in the LV tissues from these animals by detecting ROS-caused alteration of macromolecules using immunofluorescence with various ROS indicators, including 8-OHdG, a known indicator of the oxidative DNA damage, and 4HNE and MDA, the indicators of lipid peroxidation. As shown in Fig. 6D-F, all of these indicators were significantly increased in WT TAC mice compared to the sham control, indicating increased oxidative damage caused by the TAC. However, these indicators were remarkably lower in TAC TG mice compared to WT mice. These data together indicated that overexpression of VCP attenuated ROS-caused oxidative damages induced by TAC.

5. VCP regulates alternative splicing isoforms associated with heart failure.

We also conducted alternative splicing isoforms analysis to explore whether RNA splicing pattern is related to cardiac remodeling or dysfunction and will be affected by VCP. The comparisons were performed between WT and VCP TG mice at the end of the 5 W TAC. As shown in Table 3, 5 top DETXs were detected between two groups including: a spliced long non-coding RNA (lncRNA) named *myosin heavy chain associated RNA transcript (Mhrt)* and 4 coding RNAs, e.g. a transcriptional repressor named *stimulated with retinoic acid 13 (Stra13)*, a mitochondrial enzyme gene named *ATP synthase-coupling factor 6 (Atp5j)*, an ATPase gene named *ATPase Sarcoplasmic Endoplasmic Reticulum Ca2 + Transporting 2 (Serca2) or (Atp2a2)*, and a Myc-repressed gene named *N-myc downstream-regulated gene 2 (Ndr2)*, which is known as an anti-apoptotic gene in the heart. As shown in Fig. 7A-D, these DETXs presented a different profile in the alternative intron-excision options between VCP TG and WT mice at the end of the 5 W TAC.

4. Discussion

Our previous studies demonstrated an association between a decrease of the VCP expression and the hypertensive heart disease [17]. However, it is unclear whether this deficiency of VCP found in the hypertensive hearts is only an accompanying consequence of the cardiac response caused by pressure overload or is a contributor that mediates the cardiac deteriorations. We selected 5 W TAC to test the effects of VCP on pressure overload-induced heart failure for the following reasons: first, this model is an established and the most common heart failure mouse model that has been widely used to mimic human

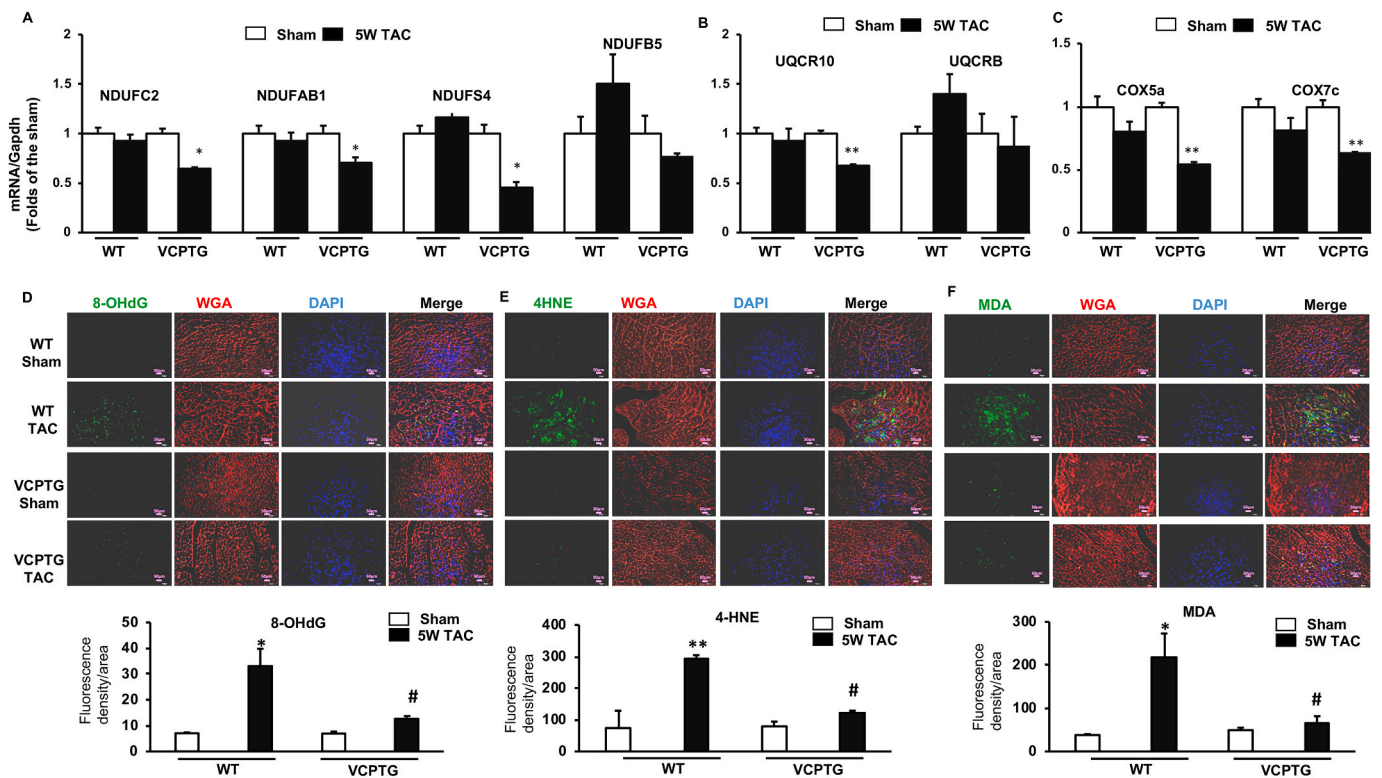


Fig. 6. VCP inhibits ROS-associated gene expression and oxidative damages under the TAC. A-C. The mRNA expression of the genes associated with mitochondrial ROS production including the subunits of mitochondrial complexes I (A), III (B) and IV (C). D-F. The representative images and quantitated indicators of ROS-caused oxidative damages in the LV tissues by the immunofluorescent staining (green) of 8-OHdG (D), 4-HNE (E) and MDA (F), combining with the Wheat Germ Agglutinin (WGA) staining (red) for cell membrane and DAPI staining (blue) for nucleic acid. **p* < 0.05, ***p* < 0.01 vs sham, #*p* < 0.05 vs corresponding WT mice. N = 3–4/groups. (For interpretation of the references to colour in this figure legend, the reader is referred to the Web version of this article.)

Table 3

DETX between VCP TG and WT at 5 W TAC.

DETX_cluster	DETX_genes	DETX_loglr	DETX_df	DETX_p.adjust
Chr14:clu_111_NA	<i>Mhrt</i>	27.1	12	0.00069
Chr16:clu_2744_NA	<i>Atp5j</i>	14.5	5	0.01326
Chr11:clu_4095_NA	<i>Stra13</i>	12.6	3	0.01311
Chr14:clu_92_NA	<i>Ndrg2</i>	11.5	3	0.01898
Chr5:clu_1545_NA	<i>Atp2a2</i>	10.7	2	0.01326

pressure-overload induced cardiac remodeling and dysfunction [31–35]. Numerous studies have confirmed that TAC could provide a reproducible model of cardiac hypertrophy, inflammatory and fibrotic response, and a gradual time course in the development of heart failure [31–34,36]. Secondly, TAC could mimic pressure-overload induced morphological and functional alterations of hypertension but excludes the impacts of other potential factors on the molecular alterations that may exist in other hypertensive models, such as the genetic and environmental effects and drug treatments. Thirdly, our previous study has shown that VCP was downregulated in both hypertensive and TAC models, and overexpression of the VCP protected the heart against cardiac hypertrophy in a model with 2 weeks TAC [17]. A 5 W TAC model would allow us to further study the role of VCP in the transition of heart from the hypertrophy to the functional failure.

Our physiological results from this study showed that overexpression of the VCP dramatically attenuated the pressure-overload-induced maladaptive cardiac remodeling and contractile dysfunction, suggesting that VCP is an essential mediator of cardiac protection against pressure overload-induced heart failure. Histological results revealed that the protection of VCP against the cardiac pathogenesis involved multiple components, including repressions of myocyte enlargement,

excessive collagen deposition and cell apoptosis. These alterations were further supported by the genomic results showing the downregulation of the related genes in VCP TG mice compared with WT upon 5 W TAC stress, providing the molecular evidence supporting physiological and histological observations in VCP TG mice. In addition, the analysis of RNA-seq results also showed that the DEGs related to the inflammation was significantly decreased in LV tissues of VCP TG mice vs WT mice at the end of 5 W TAC, indicating that VCP plays a role in inhibiting the inflammation caused by the pressure overload, which may also contribute to the cardiac protection conferred by VCP. Furthermore, GO functional analysis revealed that DEGs between VCP TG and WT mice at the end of 5 W TAC predominately related to the membrane and involved in the receptor activity of GPCR signaling pathway. These results bring a new insight in the potential mechanism that may provide cardiac protection conferred by VCP in the heart. These data, together with our previous findings, lead to a novel concept that insufficiency of VCP contributes to the pathogenesis of heart failure, and a restoration of VCP could prevent heart from the cardiac deterioration caused by pressure overload, thus, presenting a promising strategy for preventing hypertensive heart failure.

Although the differences in the cardiac structure and function between VCP TG and WT mice were observed at the end of 5 W TAC, they were not observed in the sham condition, indicating that VCP-mediated alterations are stress-associated. To determine the specific gene regulation by VCP in response to the pressure overload stress, we identified the DEGs between the 5 W TAC and sham control in either WT or VCP TG mice, respectively. The results showed that the transcriptome profiles were significantly different between VCP TG and WT mice in response to 5 W TAC when compared to their corresponding sham controls. While the genes regulating cardiac hypertrophy and fibrosis as well as inflammatory response were upregulated in WT in response to TAC, they

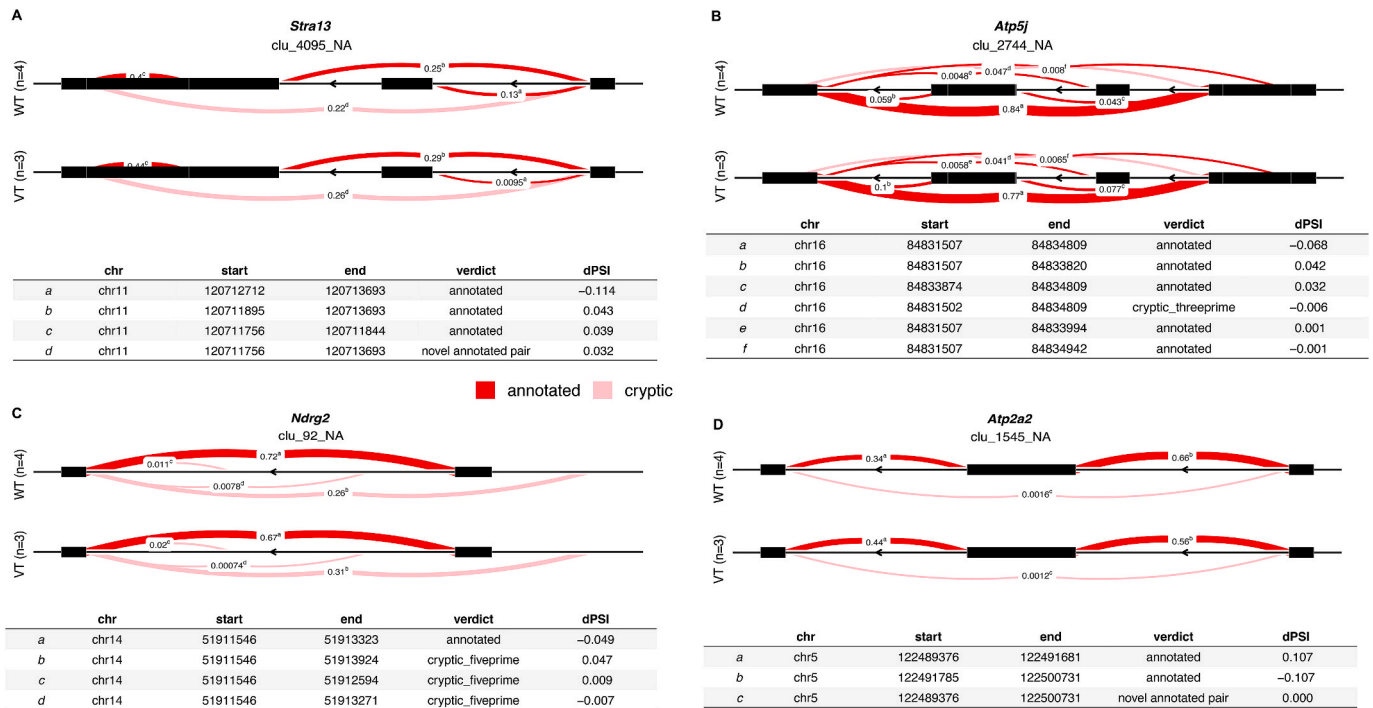


Fig. 7. VCP modulates the alternative splicing of genes in the stressed heart. LeafCutter cluster plots generated by LeafViz for DETXs detected in VCP TG vs WT mice at the end of 5 W TAC showed different modulation of alternative splicing represented by *Stra13* (A), *Atp5j*(B), *Ndr2* (C) and *Atp2a2* (D). N = 3–4 mice/group.

were downregulated in VCP TG mice. Reciprocally, the genes involved in the ER-mitochondrial function and energy metabolism were downregulated in the WT, but upregulated in VCP TG mice. In addition, the GO functional analysis also showed a distinct response to the TAC between VCP TG and WT mice. While the most of DEGs induced by the TAC were involved in the membrane that is related to GPCR signaling pathway, the predominant DEGs induced by TAC in VCP TG mice were involved in mitochondria that are related to anti-apoptosis and repressions of mitochondrial oxidative stress, transport and translation. These data may further explain the protective effects observed in VCP TG mice in inhibiting cardiac remodeling and promoting cell survival under the stress.

In addition, we found that the transcriptional factors were regulated in different manners in the VCP TG mice compared to the WT mice. *IL-10RA* is a key upstream transcriptional factor that was detected to be inhibited in WT TAC but not in VCP TG TAC mice. As a cell membrane receptor for interleukin 10, this gene mediates the immunosuppressive signal and is involved in inhibition of proinflammatory cytokines, limiting excessive tissue disruption caused by inflammation [37]. This receptor is also reported to promote cell survival through the insulin receptor substrate-2/PI 3-kinase/AKT pathway [38]. In addition, *IL10RA*-mediated activation of *STAT3* inhibits starvation-induced autophagy [39]. Thus, inhibition of *IL10RA*-mediated signaling would promote inflammation and repress cell survival in the WT TAC hearts. These findings provide a potential molecular mechanism that mediates the pressure overload-induced cardiac pathogenesis in the WT mice. This transcriptional factor-mediated signaling was preserved in VCP TG mice upon 5 W TAC, indicating that overexpression of the VCP could rectify the TAC-induced deleterious signaling. This result also further supports that inhibition of inflammatory signaling is an important mechanism of cardiac protection by VCP.

In contrast, *Rictor* was identified as a key upstream transcription factor regulating the DEGs in VCP TG mice in response to TAC. As a key adaptor, *Rictor* binds to *mTOR*, a key nutrient/energy/redox sensor and controller of protein synthesis, to constitute *mTORC2*. It has been shown that *mTORC2* plays a critical role in the phosphorylation of *AKT1* at Ser-

473, *SGK1* at Ser-422 and *PRKCA* on Ser-657 and is involved in various cellular functions [40]. *Rictor* was also found to be involved in cellular stress response and regulated cell survival in the heart through participating in the cardiac metabolisms [40]. Interestingly, in this study, we found that activation of *Rictor* in VCP TG mice upon TAC resulted in repression of most of the downstream genes that are related to ROS production [41]. This finding indicates that VCP-mediated activation of *Rictor* acts as a repressor of these oxidative stress genes. ROS was found to be increased in pressure overload-induced cardiac hypertrophy in the failing heart [42–45]. Complex I and III were considered main sites of ROS production in mitochondrial respiration chain (MRC) [46–48]. Specifically, complex I in cardiomyocytes was found to be a major source of ROS generation in pressure-overload induced LV hypertrophy and contributes to pathophysiological changes, such as the activation of redox-sensitive kinases and progression to heart failure [42,49]. It has been known that reduced abundance of MRC proteins and in particular of matrix arm subunits of complex I was associated with an improved complex I assembly, higher state 3 oxygen consumption rates and a decreased complex I-linked superoxide production [50]. Our RNA-seq data showed that, upon TAC, a group of MRC associated genes was downregulated in VCPTG mice, including the accessory (or supernumerary) subunits of complex I (*NDUFAB1*, *C2*, *S4*, *B5*) and subunits of complex III (*UQCRC10*) and complex IV (*COX5a* and *COX7c*). These alterations were further validated by qPCR data. In addition, we further revealed that overexpression of the VCP was able to protect the TG mouse hearts from ROS-caused oxidative damages induced by pressure overload, evidenced by various reduced ROS indicators in TAC TG mouse hearts compared to the WT mice at both DNA and protein levels. Together, these results indicated that VCP plays a protective role in resisting pressure overload-induced oxidative stress, which may be mediated by its modulation on the ROS production via regulating the MRC associated genes. It is well known that hypertension-induced oxidative stress plays an important role in the development of cardiac injury through ROS-mediated damages, including endothelial dysfunction, inflammation, hypertrophy, apoptosis, fibrosis and angiogenesis [51]. ROS also impairs the function of ion-channels and results in

alterations of myocyte cell calcium homeostasis, leading to impairment of contractile function and energy depletion, promoting apoptotic or necrotic cell death [52,53]. Thus, repression of these ROS-related genes in VCP TG mice may bring new insights into attenuating hypertension induced oxidative stress and promote cell survival. Our data together indicate that VCP acts as a new regulator of mTORC2 in cardiomyocytes, plays a protective effect against heart failure by repressing ROS production through the activation of *Rictor*, and subsequently, enhances the capability of the heart against the oxidative stress under pressure overload.

Finally, our results indicate a new potential role of VCP in regulating the splicing alterations of RNAs under cardiac stress, which was unrevealed previously. Alternative splicing results in multiple transcript variants encoding different isoforms, which play different roles in response to the cell stimulus. There are 5 top DETXs detected in VCP TG mice vs WT upon 5 W TAC, among which, two are involved in the repression of cell growth and hypertrophy and the other three are involved in producing ATP and cell survival. *Mhrt* is a spliced lncRNA that was detected as one of the most important DETXs in VCP TG mice. It has been shown that *Mhrt* plays a cardioprotective role in the heart by acting as a decoy to the brahma-related gene-1 (BRG1) chromatin repressor complex, preventing it from binding to its genomic targets, and subsequently, protecting the heart from pathological hypertrophy [54–56]. Regulation of the variants of this lncRNA may correlate to the protective effect of VCP against the pathogenesis of cardiac hypertrophy. Another DETX detected in the VCP TG mice is *Stra13*, a transcriptional repressor that is associated with growth arrest [57] which represses transcription through histone deacetylase (HDAC)-dependent and HDAC-independent mechanisms [58,59]. Regulation of the variants of this gene may also be responsible for the attenuation of cardiac hypertrophy conferred by VCP. These data indicate that VCP may act as a regulator across epigenomic network among the coding-genes, non-coding RNAs and HDAC in cardiac protection.

In addition, there are two other DETXs detected in VCP TG mice that were related to ATP synthesis and hydrolysis in mitochondria and are responsible for the energy metabolism in the stressed heart, including *Atp5j*, which is required for F1 and Fo interactions [60], and *Atp2a2*, a gene that encodes one of the SERCA Ca(2+)-ATPases. *Atp2a2* catalyzes the hydrolysis of ATP coupled with the translocation of calcium from the cytosol to the sarcoplasmic reticulum lumen [61,62], and is involved in calcium sequestration associated with muscular excitation and contraction [63]. These data indicate a new mechanism that VCP enhances cell survival by regulating these variants of mitochondrial genes which provide a new research interest in future research. Furthermore, *Ndr2*, a Myc-repressed gene highly expressed in heart tissue, was detected as a top DETX in VCP TG vs WT. *Ndr2* has been found to be involved in anti-apoptosis and cell survival. *NDRG2* increases in response to hypoxia-induced stress and is involved in hypoxia-induced radioresistance. It has been shown that *Ndr2* exerts protective effects against myocardial ischemia/reperfusion (I/R) injury through PI3K/Akt pathway [64,65]. It is notable that our previous studies have found that VCP interacts with AKT and increases AKT phosphorylation at Ser 473 in cardiomyocytes [16]. These results together with the new finding of this study suggest that VCP-activated AKT-associated survival signaling may be mediated by the regulation of alternative splicing of *Ndr2*, which leads to a new potential mechanism on the cardiac protection conferred by VCP in the stressed heart.

Together, our results indicate that VCP plays a key role in protecting the heart against pressure overload-induced heart failure. There are several potential mechanisms that may be involved: First, our previous study has shown that overexpression of the VCP attenuates pressure overload-induced LV hypertrophy (LVH) by inhibiting hypertrophic mTORC1 signaling [17]. Although it was a long-held view that LVH is an adaptive response to pressure overload required to sustain cardiac function, accumulating evidence from the studies in patients and animal models suggested that cardiac hypertrophy induced by chronic pressure

overload is not a compensatory but rather a maladaptive process [66, 67]. A number of TAC animal models have demonstrated that LVH is not only a predictor, but also a mediator of heart failure [1] and prevention of LVH does not lead to a dilated cardiac failure in the setting of pressure overload [1,68–70]. Our data from the current studies further showed that the overexpression of the VCP inhibits the chronic TAC-induced expressions in the genes that related to the cell growth/proliferation and inflammation. These data together indicate that increased VCP in the TG mice inhibits cardiac hypertrophy and remodeling, which interrupts the progress from hypertrophy to heart failure. Secondly, our previous studies demonstrated that VCP enhances mitochondrial function and ATP production under cardiac stress [18,71]. The reduction of VCP in WT mice under the pressure overload would impair the mitochondrial function and ATP production, which further aggravated the imbalance between the increased requirement of energy caused by the LHV and the decreased supply of ATP, leading to a reduction of contractile activity and cell damage. Our results from this study indicated that a sufficient restoration of VCP in the TG mice alters the splicing of the genes related to ATP production and the cardiac contraction, such as *Atp5j* and *Scar2*, which will help to preserve the mitochondrial energy balance under the stress and remain the cardiac contractile capability. Thirdly, our data also revealed a new potential role of VCP in inhibiting the mitochondrial ROS production under the stress, which may increase the capability of cardiomyocytes in resisting to oxidative stress caused by pressure overload, enhancing the tolerance to oxidative damage of the cells, thus promoting cell survival. The reduction of cardiac remodeling combined with increased cell survival and myocardial contractility could be beneficial to a hemodynamically challenged heart to overcome the increased after overload.

It is notable that an isoform shift in the myosin heavy chain (MHC), e.g., a decrease in alpha- (α) and an increase in beta- (β) MHC expression, has been reported in a number of models of pathologic cardiac hypertrophy and failure [72–74], nevertheless, alpha-MHC expression was found to be increased in physiological hypertrophy as observed in chronic exercise [75]. This α -to β -MHC switch, in turn, increases the expression of fetal genes such as ANP and BNP and triggers a maladaptive response. This change may also subsequently affect the transgene expression driven by the α -MHC promoter. Several transgenes have been reported to be downregulated under the pressure-overload induced heart failure that may be due to a reduction of α -MHC expression [76, 77], however, such influence in the transgene expression was not observed in other genes [78–80]. The mechanisms of these differences are not fully understood, but may be associated with the time and status of the pathological alterations, the nature of the target genes, insertional effects and the influence of additional regulatory elements. Our results showed that VCP was not significantly altered in the 5 W TAC mouse heart when compared to their sham controls. The preserved expression of the VCP was confirmed at both mRNA and protein levels, indicating that α -MHC remains to be the predominant isoform in the VCP TG heart. Our data also showing no increase in the fetal genes (ANP and BNP) in the VCP TAC mice further support this possibility. Although the mechanisms remain to be further investigated, there are several possibilities that may be involved in the preservation of VCP expression in the TG mice during TAC. First, an α -to β -MHC switch was found to be highly associated with pathological hypertrophy and failing heart. Our previous study showed that overexpression of the VCP prevents pressure overload-induced pathological hypertrophy [17], which may also contribute to the preservation of VCP expression. Secondly, it has been shown that the regulation of MHC gene expression during hypertrophy is complex, as both transcriptional and post-transcriptional regulatory mechanisms have been shown to play a role [75]. VCP-mediated signaling may involve a regulation of MHC gene expression during hypertrophy with an attenuated α -to β -MHC switch. While VCP was downregulated in the 5 W TAC in WT mice, VCP TG mice could restore the substantial loss of VCP which was sufficient to abolish the pressure overload-induced deleterious signaling and to maintain functional

activity. In addition, it has been shown that VCP mediates its downstream signaling by interacting with various co-factors, inducing a combinatorial gene control, which makes it possible to generate considerable biological complexity with a relatively defined number of regulatory molecules under the stress.

In summary, our data suggested that VCP acted as a novel mediator of cardiac protection against pressure overload-induced heart failure, which may involve a comprehensive genomic networks, including rectifying stress-induced pathological hypertrophic and inflammatory signaling, enhancing the anti-oxidative stress and modulation of alternative splicing of genes in cell growth and mitochondrial function (abstract figure).

Data and code availability

Our RNA-seq fastq files were submitted to GEO with the access number (GSE134085). The dataset will be available as soon as our manuscript is accepted for a publication.

Authors contributions

HQ designed the study. CW and NZ performed RNA-seq experiment and obtained RNA-seq data. XC performed bioinformatics data analysis. NZ performed the surgeries and physiological measurements as well as RNA extraction. BM, CL and SS performed qPCR, histological studies and data analysis. HQ, CW, XC, JX, NZ, and GQ drafted and revised the manuscript. GQ helped the annotations. All authors reviewed the final version of the manuscript, and agreed with the content and ensured the accuracy and integrity of the results in the manuscript.

Declaration of competing interest

All the authors have no conflict of interest.

Acknowledgements

This work is supported by NIH grants HL115195 (H.Q.), HL137962 (H.Q.), and HL 142291(H.Q. & G.Q). We would also like to thank the partial support from the Ardmore Institute of Health (AIH) grant (2150141, CW), the National Natural Science Foundation of China 81570261 (N.Z.) and Dr. Charles A. Sims' gift to Loma Linda University (LLU) Center for Genomics.

References

[1] M.H. Drazner, The progression of hypertensive heart disease, *Circulation* 123 (3) (2011) 327–334.

[2] A.A. Soenarta, P. Buranakitjaroen, Y.C. Chia, C.H. Chen, J. Naites, S. Hoshida, H. V. Minh, S. Park, J. Shin, S. Siddique, et al., An overview of hypertension and cardiac involvement in Asia: focus on heart failure, *J. Clin. Hypertens.* 22 (3) (2020) 423–430.

[3] G.C. Oh, H.J. Cho, Blood pressure and heart failure, *Clin Hypertens* 26 (2020) 1.

[4] W.B. Kannel, J. Cobb, Left ventricular hypertrophy and mortality—results from the Framingham Study, *Cardiology* 81 (4–5) (1992) 291–298.

[5] M. Santos, A.M. Shah, Alterations in cardiac structure and function in hypertension, *Curr. Hypertens. Rep.* 16 (5) (2014) 428.

[6] K. Dharmarajan, M.W. Rich, Epidemiology, pathophysiology, and prognosis of heart failure in older adults, *Heart Fail. Clin.* 13 (3) (2017) 417–426.

[7] W.K. Tang, D. Xia, Mutations in the human AAA+ chaperone p97 and related diseases, *Front. Mol. Biosci.* 3 (2016) 79.

[8] H. Niwa, C.A. Ewens, C. Tsang, H.O. Yeung, X. Zhang, P.S. Freemont, The role of the N-domain in the ATPase activity of the mammalian AAA ATPase p97/VCP, *J. Biol. Chem.* 287 (11) (2012) 8561–8570.

[9] H. Meyer, C.C. Wehl, The VCP/p97 system at a glance: connecting cellular function to disease pathogenesis, *J. Cell Sci.* 127 (Pt 18) (2014) 3877–3883.

[10] S. Yamamoto, Y. Tomita, T. Uruno, Y. Hoshida, Y. Qiu, N. Iizuka, I. Nakamichi, A. Miyachi, K. Aozasa, Increased expression of valosin-containing protein (p97) is correlated with disease recurrence in follicular thyroid cancer, *Ann. Surg. Oncol.* 12 (11) (2005) 925–934.

[11] S. Yamamoto, Y. Tomita, Y. Hoshida, N. Iizuka, M. Monden, S. Yamamoto, K. Iuchi, K. Aozasa, Expression level of valosin-containing protein (p97) is correlated with

progression and prognosis of non-small-cell lung carcinoma, *Ann. Surg. Oncol.* 11 (7) (2004) 697–704.

[12] B. Lan, S. Chai, P. Wang, K. Wang, VCP/p97/Cdc48, A linking of protein homeostasis and cancer therapy, *Curr. Mol. Med.* 17 (9) (2017) 608–618.

[13] V. Kimonis, Inclusion body myopathy with paget disease of bone and/or frontotemporal dementia, in: M.P. Adam, H.H. Ardinger, R.A. Pagon, S.E. Wallace, L.J.H. Bean, K. Stephens, A. Amemiya (Eds.), *GeneReviews(R)*, 1993. Seattle (WA).

[14] M.J. Brody, D. Vanhoutte, C.V. Bakshi, R. Liu, R.N. Correll, M.A. Sargent, J. D. Molkentin, Disruption of valosin-containing protein activity causes cardiomyopathy and reveals pleiotropic functions in cardiac homeostasis, *J. Biol. Chem.* 294 (22) (2019) 8918–8929.

[15] M.C. Viswanathan, A.C. Blice-Baum, T.K. Sang, A. Cammarato, Cardiac-restricted expression of VCP/TER94 RNAi or disease alleles perturbs *Drosophila* heart structure and impairs function, *J. Cardiovasc. Dev. Dis.* 3 (2) (2016).

[16] P. Lizano, E. Rashed, H. Kang, H. Dai, X. Sui, L. Yan, H. Qiu, C. Depre, The valosin-containing protein promotes cardiac survival through the inducible isoform of nitric oxide synthase, *Cardiovasc. Res.* 99 (4) (2013) 685–693.

[17] N. Zhou, B. Ma, S. Stoll, T.T. Hays, H. Qiu, The valosin-containing protein is a novel repressor of cardiomyocyte hypertrophy induced by pressure overload, *Aging Cell* 16 (5) (2017) 1168–1179.

[18] P. Lizano, E. Rashed, S. Stoll, N. Zhou, H. Wen, T.T. Hays, G. Qin, L.H. Xie, C. Depre, H. Qiu, The valosin-containing protein is a novel mediator of mitochondrial respiration and cell survival in the heart in vivo, *Sci. Rep.* 7 (2017) 46324.

[19] H. Qiu, P. Lizano, L. Laure, X. Sui, E. Rashed, J.Y. Park, C. Hong, S. Gao, E. Holle, D. Morin, et al., H11 kinase/heat shock protein 22 deletion impairs both nuclear and mitochondrial functions of STAT3 and accelerates the transition into heart failure on cardiac overload, *Circulation* 124 (4) (2011) 406–415.

[20] G.Y. Liou, P. Storz, Detecting reactive oxygen species by immunohistochemistry, *Methods Mol. Biol.* 1292 (2015) 97–104.

[21] K.K. Griendling, R.M. Touyz, J.L. Zweier, S. Dikalov, W. Chilian, Y.R. Chen, D. G. Harrison, A. Bhatnagar, American heart association council on basic cardiovascular S: measurement of reactive oxygen species, reactive nitrogen species, and redox-dependent signaling in the cardiovascular system: a scientific statement from the American heart association, *Circ. Res.* 119 (5) (2016) e39–75.

[22] M. Dhiman, M.P. Zago, S. Nunez, A. Amoroso, H. Rementeria, P. Dousset, F. Nunez Burgos, N.J. Garg, Cardiac-oxidized antigens are targets of immune recognition by antibodies and potential molecular determinants in chagas disease pathogenesis, *PloS One* 7 (1) (2012), e28449.

[23] A. Buchberger, H. Schindelin, P. Hanzelmann, Control of p97 function by cofactor binding, *FEBS Lett.* 589 (19 Pt A) (2015) 2578–2589.

[24] A.M. Bolger, M. Lohse, B. Usadel, Trimmomatic: a flexible trimmer for Illumina sequence data, *Bioinformatics* 30 (15) (2014) 2114–2120.

[25] C.C. Lo, P.S. Chain, Rapid evaluation and quality control of next generation sequencing data with FaQCs, *BMC Bioinf.* 15 (2014) 366.

[26] X. Gao, D. Hu, M. Gogol, H. Li, ClusterMap: compare multiple Single Cell RNA-Seq datasets across different experimental conditions, *Bioinformatics* 35 (17) (2019) 3038–3045.

[27] D. Tabas-Madrid, R. Nogales-Cadenas, A. Pascual-Montano, GeneCodis3: a non-redundant and modular enrichment analysis tool for functional genomics, *Nucleic Acids Res.* 40 (2012). Web Server issue:W478–483.

[28] R. Nogales-Cadenas, P. Carmona-Saez, M. Vazquez, C. Vicente, X. Yang, F. Tirado, J.M. Carazo, A. Pascual-Montano, GeneCodis: interpreting gene lists through enrichment analysis and integration of diverse biological information, *Nucleic Acids Res.* 37 (2009). Web Server issue:W317–322.

[29] P. Carmona-Saez, M. Chagoyen, F. Tirado, J.M. Carazo, A. Pascual-Montano, GENECODIS: a web-based tool for finding significant concurrent annotations in gene lists, *Genome Biol.* 8 (1) (2007) R3.

[30] Y.I. Li, D.A. Knowles, J. Humphrey, A.N. Barbeira, S.P. Dickinson, H.K. Im, J. K. Pritchard, Annotation-free quantification of RNA splicing using LeafCutter, *Nat. Genet.* 50 (1) (2018) 151–158.

[31] H. Lin, Y. Li, H. Zhu, Q. Wang, Z. Chen, L. Chen, Y. Zhu, C. Zheng, Y. Wang, W. Liao, et al., Lansoprazole alleviates pressure overload-induced cardiac hypertrophy and heart failure in mice by blocking the activation of beta-catenin, *Cardiovasc. Res.* 116 (1) (2020) 101–113.

[32] M.M. Sung, S.K. Das, J. Levasseur, N.J. Byrne, D. Fung, T.T. Kim, G. Masson, J. Boisvenue, C.L. Soltys, G.Y. Oudit, et al., Resveratrol treatment of mice with pressure-overload-induced heart failure improves diastolic function and cardiac energy metabolism, *Circ. Heart Fail* 8 (1) (2015) 128–137.

[33] A.C. deAlmeida, R.J. van Oort, X.H. Wehrens, Transverse aortic constriction in mice, *JoVE* 38 (2010).

[34] J. Yoo, V. Chepurko, R.J. Hajjar, D. Jeong, Conventional method of transverse aortic constriction in mice, *Methods Mol. Biol.* 1816 (2018) 183–193.

[35] R. Breckenridge, Heart failure and mouse models, *Dis. Model. Mech.* 3 (3–4) (2010) 138–143.

[36] Y. Xia, K. Lee, N. Li, D. Corbett, L. Mendoza, N.G. Frangogiannis, Characterization of the inflammatory and fibrotic response in a mouse model of cardiac pressure overload, *Histochem. Cell Biol.* 131 (4) (2009) 471–481.

[37] S.I. Yoon, N.J. Logsdon, F. Sheikh, R.P. Donnelly, M.R. Walter, Conformational changes mediate interleukin-10 receptor 2 (IL-10R2) binding to IL-10 and assembly of the signaling complex, *J. Biol. Chem.* 281 (46) (2006) 35088–35096.

[38] A. Usacheva, S. Kotenko, M.M. Witte, O.R. Colamonici, Two distinct domains within the N-terminal region of Janus kinase 1 interact with cytokine receptors, *J. Immunol.* 169 (3) (2002) 1302–1308.

- [39] J. Shi, H. Wang, H. Guan, S. Shi, Y. Li, X. Wu, N. Li, C. Yang, X. Bai, W. Cai, et al., IL10 inhibits starvation-induced autophagy in hypertrophic scar fibroblasts via cross talk between the IL10-IL10R-STAT3 and IL10-AKT-mTOR pathways, *Cell Death Dis.* 7 (2016) e2133.
- [40] S. Sciarretta, M. Forte, G. Frati, J. Sadoshima, New insights into the role of mTOR signaling in the cardiovascular system, *Circ. Res.* 122 (3) (2018) 489–505.
- [41] P. Puddu, G.M. Puddu, E. Cravero, M. Rosati, A. Muscari, The molecular sources of reactive oxygen species in hypertension, *Blood Press.* 17 (2) (2008) 70–77.
- [42] M. Schwarzer, M. Osterholt, A. Lunkenbein, A. Schreppler, P. Amorim, T. Doenst, Mitochondrial reactive oxygen species production and respiratory complex activity in rats with pressure overload-induced heart failure, *J. Physiol.* 592 (17) (2014) 3767–3782.
- [43] C.M. Sag, C.X. Santos, A.M. Shah, Redox regulation of cardiac hypertrophy, *J. Mol. Cell. Cardiol.* 73 (2014) 103–111.
- [44] J. Yang, S. Wu, L. Zhu, J. Cai, L. Fu, Hydrogen-containing saline alleviates pressure overload-induced interstitial fibrosis and cardiac dysfunction in rats, *Mol. Med. Rep.* 16 (2) (2017) 1771–1778.
- [45] M. Maytin, D.A. Siwik, M. Ito, L. Xiao, D.B. Sawyer, R. Liao, W.S. Colucci, Pressure overload-induced myocardial hypertrophy in mice does not require gp91phox, *Circulation* 109 (9) (2004) 1168–1171.
- [46] M.P. Murphy, How mitochondria produce reactive oxygen species, *Biochem. J.* 417 (1) (2009) 1–13.
- [47] D.B. Zorov, M. Juhaszova, S.J. Sollott, Mitochondrial reactive oxygen species (ROS) and ROS-induced ROS release, *Physiol. Rev.* 94 (3) (2014) 909–950.
- [48] L. Bleier, S. Drose, Superoxide generation by complex III: from mechanistic rationales to functional consequences, *Biochim. Biophys. Acta* 1827 (11–12) (2013) 1320–1331.
- [49] J.M. Li, N.P. Gall, D.J. Grieve, M. Chen, A.M. Shah, Activation of NADPH oxidase during progression of cardiac hypertrophy to failure, *Hypertension* 40 (4) (2002) 477–484.
- [50] S. Miwa, H. Jow, K. Baty, A. Johnson, R. Czapiewski, G. Saretzki, A. Treumann, T. von Zglinicki, Low abundance of the matrix arm of complex I in mitochondria predicts longevity in mice, *Nat. Commun.* 5 (2014) 3837.
- [51] A. Csiszar, P. Pacher, G. Kaley, Z. Ungvari, Role of oxidative and nitrosative stress, longevity genes and poly(ADP-ribose) polymerase in cardiovascular dysfunction associated with aging, *Curr. Vasc. Pharmacol.* 3 (3) (2005) 285–291.
- [52] L.M. Bendhack, R.V. Sharma, R.C. Bhalla, Altered signal transduction in vascular smooth muscle cells of spontaneously hypertensive rats, *Hypertension* 19 (2 Suppl) (1992) III42–148.
- [53] E. Bartha, I. Solti, L. Kereskai, J. Lantos, E. Plozer, K. Magyar, E. Szabados, T. Kalai, K. Hideg, R. Halmosi, et al., PARP inhibition delays transition of hypertensive cardiopathy to heart failure in spontaneously hypertensive rats, *Cardiovasc. Res.* 83 (3) (2009) 501–510.
- [54] H. Zhou, B. Wang, Y.X. Yang, Q.J. Jia, A. Zhang, Z.W. Qi, J.P. Zhang, Long noncoding RNAs in pathological cardiac remodeling: a review of the update literature, *BioMed Res. Int.* 2019 (2019) 7159592.
- [55] Y. Luo, Y. Xu, C. Liang, W. Xing, T. Zhang, The mechanism of myocardial hypertrophy regulated by the interaction between mhrnt and myocardin, *Cell. Signal.* 43 (2018) 11–20.
- [56] S. Uchida, S. Dimmeler, Long noncoding RNAs in cardiovascular diseases, *Circ. Res.* 116 (4) (2015) 737–750.
- [57] S. Azmi, R. Taneja, Embryonic expression of mSharp-1/mDEC2, which encodes a basic helix-loop-helix transcription factor, *Mech. Dev.* 114 (1–2) (2002) 181–185.
- [58] H. Sun, R. Taneja, Stra13 expression is associated with growth arrest and represses transcription through histone deacetylase (HDAC)-dependent and HDAC-independent mechanisms, *Proc. Natl. Acad. Sci. U. S. A.* 97 (8) (2000) 4058–4063.
- [59] S.V. Ivanov, K. Salnikow, A.V. Ivanova, L. Bai, M.I. Lerman, Hypoxic repression of STAT1 and its downstream genes by a pVHL/HIF-1 target DEC1/STRA13, *Oncogene* 26 (6) (2007) 802–812.
- [60] H.W. Wang, W.P. Zhao, J. Liu, P.P. Tan, W.S. Tian, B.H. Zhou, ATP5J and ATP5H proactive expression correlates with cardiomyocyte mitochondrial dysfunction induced by fluoride, *Biol. Trace Elem. Res.* 180 (1) (2017) 63–69.
- [61] L. Zhihao, N. Jingyu, L. Lan, S. Michael, G. Rui, B. Xiyun, L. Xiaozhi, F. Guanwei, SERCA2a: a key protein in the Ca(2+) cycle of the heart failure, *Heart Fail. Rev.* 25 (3) (2020) 523–535.
- [62] S. Li, A. Chopra, W. Keung, C.W.Y. Chan, K.D. Costa, C.W. Kong, R.J. Hajjar, C. S. Chen, R.A. Li, Sarco/endoplasmic reticulum Ca(2+)-ATPase is a more effective calcium remover than sodium-calcium exchanger in human embryonic stem cell-derived cardiomyocytes, *Am. J. Physiol. Heart Circ. Physiol.* 317 (5) (2019) H1105–H1115.
- [63] M. Periasamy, S. Huke, SERCA pump level is a critical determinant of Ca(2+) homeostasis and cardiac contractility, *J. Mol. Cell. Cardiol.* 33 (6) (2001) 1053–1063.
- [64] Z. Sun, G. Tong, N. Ma, J. Li, X. Li, S. Li, J. Zhou, L. Xiong, F. Cao, L. Yao, et al., NDRG2: a newly identified mediator of insulin cardioprotection against myocardial ischemia-reperfusion injury, *Basic Res. Cardiol.* 108 (3) (2013) 341.
- [65] Z. Sun, L. Shen, X. Sun, G. Tong, D. Sun, T. Han, G. Yang, J. Zhang, F. Cao, L. Yao, et al., Variation of NDRG2 and c-Myc expression in rat heart during the acute stage of ischemia/reperfusion injury, *Histochem. Cell Biol.* 135 (1) (2011) 27–35.
- [66] B.C. Bernardo, K.L. Weeks, L. Pretorius, J.R. McMullen, Molecular distinction between physiological and pathological cardiac hypertrophy: experimental findings and therapeutic strategies, *Pharmacol. Ther.* 128 (1) (2010) 191–227.
- [67] W. Nadruz, Myocardial remodeling in hypertension, *J. Hum. Hypertens.* 29 (1) (2015) 1–6.
- [68] G. Esposito, A. Rapacciuolo, S.V. Naga Prasad, H. Takaoka, S.A. Thomas, W. J. Koch, H.A. Rockman, Genetic alterations that inhibit in vivo pressure-overload hypertrophy prevent cardiac dysfunction despite increased wall stress, *Circulation* 105 (1) (2002) 85–92.
- [69] J.A. Hill, M. Karimi, W. Kutschke, R.L. Davisson, K. Zimmerman, Z. Wang, R. E. Kerber, R.M. Weiss, Cardiac hypertrophy is not a required compensatory response to short-term pressure overload, *Circulation* 101 (24) (2000) 2863–2869.
- [70] N. Frey, H.A. Katus, E.N. Olson, J.A. Hill, Hypertrophy of the heart: a new therapeutic target? *Circulation* 109 (13) (2004) 1580–1589.
- [71] S. Stoll, J. Xi, B. Ma, C. Leimena, E.J. Behringer, G. Qin, H. Qiu, The valosin-containing protein protects the heart against pathological Ca2+ overload by modulating Ca2+ uptake proteins, *Toxicol. Sci.* 171 (2) (2019) 473–484.
- [72] S. Besse, P. Assayag, C. Delcayre, F. Carre, S.L. Cheav, Y. Lecarpentier, B. Swynghedauw, Normal and hypertrophied senescent rat heart: mechanical and molecular characteristics, *Am. J. Physiol.* 265 (1 Pt 2) (1993) H183–H190.
- [73] M.O. Boluyt, L. O'Neill, A.L. Meredith, O.H. Bing, W.W. Brooks, C.H. Conrad, M. T. Crow, E.G. Lakatta, Alterations in cardiac gene expression during the transition from stable hypertrophy to heart failure. Marked upregulation of genes encoding extracellular matrix components, *Circ. Res.* 75 (1) (1994) 23–32.
- [74] B.D. Lowes, W. Minobe, W.T. Abraham, M.N. Rizeq, T.J. Bohlmeier, R.A. Quaife, R.L. Roden, D.L. Dutcher, A.D. Robertson, N.F. Voelkel, et al., Changes in gene expression in the intact human heart. Downregulation of alpha-myosin heavy chain in hypertrophied, failing ventricular myocardium, *J. Clin. Invest.* 100 (9) (1997) 2315–2324.
- [75] M.P. Gupta, Factors controlling cardiac myosin-isoform shift during hypertrophy and heart failure, *J. Mol. Cell. Cardiol.* 43 (4) (2007) 388–403.
- [76] D.J. Sheridan, D.J. Autelitano, B. Wang, E. Percy, E.A. Woodcock, X.J. Du, Beta(2)-adrenergic receptor overexpression driven by alpha-MHC promoter is downregulated in hypertrophied and failing myocardium, *Cardiovasc. Res.* 47 (1) (2000) 133–141.
- [77] U. Mende, A. Kagen, A. Cohen, J. Aramburu, F.J. Schoen, E.J. Neer, Transient cardiac expression of constitutively active Galphaq leads to hypertrophy and dilated cardiomyopathy by calcineurin-dependent and independent pathways, *Proc. Natl. Acad. Sci. U. S. A.* 95 (23) (1998) 13893–13898.
- [78] K. Kazmierczak, C.C. Yuan, J. Liang, W. Huang, A.I. Rojas, D. Szczesna-Cordary, Remodeling of the heart in hypertrophy in animal models with myosin essential light chain mutations, *Front. Physiol.* 5 (2014) 353.
- [79] K.N. Lee, X. Lu, C. Nguyen, Q. Feng, P. Chidiac, Cardiomyocyte specific overexpression of a 37 amino acid domain of regulator of G protein signalling 2 inhibits cardiac hypertrophy and improves function in response to pressure overload in mice, *J. Mol. Cell. Cardiol.* 108 (2017) 194–202.
- [80] C. Chen, R. Huo, Y. Tong, Y. Sheng, H.B. Liu, X. Gao, O. Nakajima, B.F. Yang, D. L. Dong, Systemic heme oxygenase-1 transgenic overexpression aggravates pressure overload-induced cardiac hypertrophy in mice, *Cell. Physiol. Biochem.* 28 (1) (2011) 25–32.